Development of a medium-energy superconducting heavy-ion linac

P. N. Ostroumov
Physics Division, Argonne National Laboratory, 9700 S. Cass Avenue, Argonne, Illinois 60439
(Received 25 January 2002; published 25 March 2002)

The Rare Isotope Accelerator (RIA) facility project includes a cw 1.4 GeV driver linac and a 100 MV postaccelerator both based on superconducting (SC) cavities operating at frequencies from 48 to 805 MHz. In these linacs more than 99% of the total voltage is provided by SC cavities. An initial acceleration is provided by room temperature radio frequency quadrupoles. The driver linac is designed for acceleration of any ion species, from protons up to 900 MeV to uranium up to 400 MeV/u. The novel feature of the driver linac is an acceleration of multiple charge-state heavy-ion beams in order to achieve 400 kW beam power. This paper presents design features of a medium-energy SC heavy-ion linac taking the RIA driver linac as an example. The dynamics of single and multiple charge-state beams are detailed, including the effects of possible errors in rf field parameters and misalignments of transverse focusing elements. The important design considerations of such linac are presented. Several new conceptual solutions in beam dynamics in SC accelerating structures for heavy-ion applications are discussed.

DOI: 10.1103/PhysRevSTAB.5.030101 PACS numbers: 29.17.+w, 29.27.-a, 41.75.-i

I. GENERAL LAYOUT OF SC MEDIUM-ENERGY LINAC

The principal requirements for a high-power medium-energy superconducting (SC) accelerator are that it be capable of producing beams of any ion, including uranium, at energies of 400 MeV/nucleon and a total beam power of 400 kW. A conceptual design for such a linac has been developed for the Rare Isotope Accelerator (RIA) project, the major elements of which are shown in Fig. 1. The beam energies shown in Fig. 1 are for the benchmark uranium beam. Except for the injector radio frequency quadrupole (RFQ), the entire linac is based on SC accelerating structures, which not only enable cost-effective cw operation, but also, as discussed below, have numerous additional advantages for this application. The linac will contain nine types of superconducting radio frequency (SRF) accelerating cavities. The layout, configuration, and many details of the RIA driver linac have been discussed and presented at several conferences and workshops [1–5].

Superconducting ion linacs are configured as an array of short superconducting cavities, each with an independently controllable rf phase. Independent phasing allows the velocity profile to be varied: the linac can be tuned to provide higher energies for the lighter ions. For example, the reference design linac can be tuned to provide a uranium beam at an energy of 403 MeV/u and can be retuned to provide a proton beam at 899 MeV. To obtain 403 MeV/u of uranium beam the driver linac has to have two strippers. Three different sections of the linac are demarked by the charge strippers. The low-β section of the linac is that portion prior to the first stripper, the medium-β section is that between the two strippers, and the high-β section is that portion following the second stripper. The low- and medium-β sections employ drift-tube class cavities, and the high-β section, elliptical cell cavities.

The longitudinal and transverse acceptance of the high-β section is $\sim$100 times larger than the input beam emittance, which is determined by the ion source and injector RFQ. Such an immense margin for emittance growth makes possible a novel operating mode for the linac, in which the beam contains multiple charge states [6,7]. By simultaneously accelerating several of the multiple charge states resulting from stripping the beam, a much higher portion of the stripped beam can be utilized. The increase in efficiency not only provides a substantial increase in the available beam current, but also enables the use of multiple strippers, reducing the size of the linac required for 400 MeV/u beams. A third benefit of using multiple charge states is a reduction in the amount of beam dumped during the charge-state selection at the stripping points: this in turn reduces shielding requirements. As discussed in Refs. [6,7], full 3D numerical simulations show such an operation to be straightforward, entailing a modest increase of longitudinal and transverse emittance, which remains well within the linac acceptance. Also, it should be

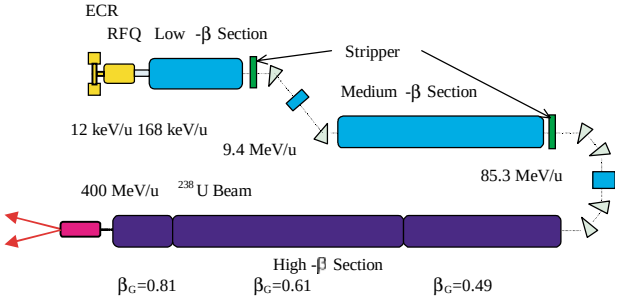

FIG. 1. (Color) Elements of the proposed linac.

 © 2002 The American Physical Society

noted that the feasibility of multiple charge-state (multi-q) beam acceleration has been experimentally established in a series of tests with the existing SC ion accelerator ATLAS [8,9]. In addition, it was shown that the front end of the driver linac can be designed for the acceptance of two charge states of uranium beam from the electron cyclotron resonance (ECR) ion source, doubling the available uranium beam power [10].

The driver linac is a high intensity machine and relative beam losses in the high-energy section must be kept below 10^{-4}. Acceleration of the multi-q uranium beam places stringent requirements on the linac design. Any other lighter ion beams can be accelerated with much smaller emittances. Below we present beam dynamics studies which have been performed with the goal of optimization of the linac structure in order to reduce a possible effective emittance growth of the multi-q uranium beam.

In the low- and medium-β sections of the driver linac intercryostat spaces can affect beam dynamics substantially. Several important measures will be applied in order to minimize the length of the intercryostat spaces and to facilitate an impact of the drift spaces on the beam dynamics.

(i) The RFQ and multiharmonic buncher are specially designed in order to provide very low longitudinal emittance of a two charge-state uranium beam.

(ii) Intercryostat space will contain only vacuum valves and a beam profile monitor. These devices will be designed for the lowest possible space occupation along the beam line.

(iii) Beam steering coils will be combined with the SC focusing solenoids and will not require an additional space along the beam line.

(iv) Standard accelerating SRF cavities can be switched to the mode of a beam phase monitor in order to set up phases and amplitudes of the accelerating fields in the upstream cavities. No space is required for beam phase monitors between the cryostats.

(v) Transverse matching between the cryostats is facilitated by the absence of the first SRF cavity in the very first focusing period of the cryostats.

(vi) A special transition section is designed between the first two cryostats of low-β linac where beam energy is low and beam matching is extremely critical to the length of the drift space.

II. LINAC DESIGN CODES

Several computer codes were applied for the design of the driver linac. Beam parameters of ECR ion sources were adopted from the recent experimental data and extrapolation to higher intensities on the basis of estimates of the VENUS Ion Source group [11]. For the design of low-energy beam transport lines the codes GIOS [12], COSY [13], and DYNAMION [14] were used. The RFQ capable of accelerating a two charge-state uranium beam was designed using the DYNAMION code [10]. Beam dynamics design and optimization along the SRF linac was performed by the TRACK code [15]. Beam transport codes including higher order terms such as TRANSPORT [16], GIOS, and COSY were applied for the design of multi-q beam transitions and switchyards.

The code TRACK has been written in order to integrate charged particle motion in the presence of all components of the electromagnetic field. The electromagnetic fields in all types of SRF cavities were obtained from the code CST Microwave Studio (MWS) [17]. The TRACK code simulates multiparticle motion in six-dimensional phase space on the base of an iterative solution of the equation of motion [15]. The MWS code running on modern PCs can calculate all six components of electromagnetic field distribution within the beam-cavity interaction area with a mesh size less than 1 mm.

The simulation of beam dynamics in the presence of all components of both electric and magnetic fields is essential in superconducting quarter-wave resonators (QWR). The driver linac will use more than 85 QWRs operating at 57.5 and 115 MHz. Electrodynamics studies of the field distributions in the beam-cavity interaction area indicate appreciable dipole components of both electric and magnetic fields, especially for higher frequency cavities. The dipole fields induce beam steering, which is a strong function of the rf phase and which couples the longitudinal and transverse motion resulting in transverse emittance growth. Such emittance growth cannot be compensated by static fields and can be a particularly serious problem in applications for beams with a high charge-to-mass ratio. For example, the low-β section of the driver linac can be retuned to provide a maximum energy gain of 45.8 MeV for protons. This regime is most sensitive to beam steering by the dipole components of the electromagnetic field. We have analyzed and proposed two possible methods for the correction of such dynamic beam steering effects in quarter-wave resonators [15]. As was shown, a complete compensation of the steering effect can be largely eliminated by shaping the drift-tube and cavity-wall faces adjacent to the beam axis to provide appropriate corrective vertical electric field components. This method can correct steering of proton beams over the entire velocity range where QWRs are applicable.

Beam dynamics simulation in each of three sections of the driver linac included the following steps.

(i) Beam matching in transverse and longitudinal phase spaces for a trial beam with the mean value of charge-to-mass ratio. Simulation of the trial ion beam to minimize beam sizes and to obtain smooth rms envelopes in transverse planes. The rms oscillations in longitudinal phase space due to the effect of intercavity drift spaces were minimized but not eliminated completely. In the parts of the linac the synchronous phase is equal to -30°, which produces a large linear region for the beam size oscillations. Therefore the longitudinal emittance of the trial beam does not grow.

(ii) Simulation of the multi-q beam. Final determination of beam energies at stripping foil and total required number of the cavities.

(iii) Beam dynamics simulation of the multi-q beam under the effect of random errors both in transverse and longitudinal phase space.

III. LOW-β LINAC

This section accelerates uranium ions from 170 keV/u to 9.4 MeV/u. Lighter ions can be accelerated to higher energies by retuning the phase setting of the accelerating cavities as mentioned in the previous section of this paper. Table I shows basic parameters of the accelerating and focusing lattice of the low-β linac section. It consists of an array of 85 SC cavities distributed in ten cryostat modules. Transverse focusing is provided by SC solenoids contained in the same cryostat modules as the cavities. The low-β linac will start with a lattice of a solenoid with each cavity and finish with one solenoid per three cavities. Such an array, with the cavities operated at a synchronous phase $\varphi_S = -30°$, provides strong focusing in both transverse and longitudinal phase space. Because of the strong damping of the bunch phase width as beam energy is increased, the 115 MHz SRF cavities can be set at a synchronous phase $\varphi_S = -25°$. Prior to numerical ray tracing a two charge-state beam through the low-β section, the transverse beam motion was matched carefully using fitting codes for a trial beam of charge state $q = 28.5$. A particularly critical aspect of fitting was to avoid beam mismatch at the transitions between focusing periods of differing lengths and between the cryostats. Note that the focusing lattice length is different for each of the four types of SRF cavities. Beam dynamics in the SRF linac were numerically simulated using the TRACK code [15].

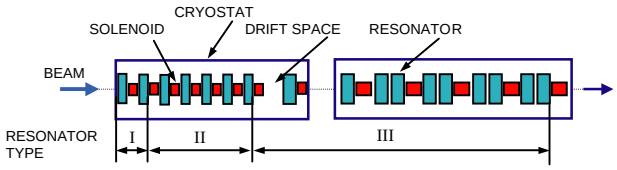

FIG. 2. (Color) Layout of the first two cryostats of the low-β linac.

The preprocessor code generates the phase setting for the uranium beam with an average charge state $q = 28.5$.

Beam mismatch in both transverse and longitudinal phase space is a critical issue in the drift space between the first two cryostats where the beam energy is low ~700 keV/u. The matching between these two cryostats is performed by the help of a specially designed transition section shown in Fig. 2. The last cavity in cryostat 1 is a 2-gap QWR (type III, see Table I) tuned for $-40°$ synchronous phase in order to create a time focus at the entrance of the second cryostat. The drift space between the first two cryostat is set to be 60 cm which is sufficient to install end covers of the cryostats, vacuum valves, and several units of beam instrumentation.

The cryostat structures containing two types of SRF cavities are shown in Fig. 3. The focusing period of the cryostat contains two 57.5 MHz cavities per period except for the first period which forms a focusing period with a "missing" cavity. The space of the missed cavity is replaced by the intercryostat drift. The flange-to-flange distance between the elements located in adjacent cryostats is set to be 40 cm. The focusing structure with the missing cavity is extremely helpful for the tuning of the beam motion in the transverse phase space. A little adjustment of the focusing fields in the outermost solenoids is required in order to match the beam. A similar focusing structure

TABLE I. Basic parameters of the low-β linac section.

Beam energy, MeV/u	0.17–0.32	0.32–0.77	0.77–4.35	4.35–9.43
Frequency (MHz)	57.5	57.5	57.5	115
Number of cavities per focusing period	1	1	2	3
Number of cavities	2	5	37	41
Number of cryostats		1	4	5
Type of cavity	4-gap, $\lambda/4$ type I	4-gap, $\lambda/4$ type II	2-gap, $\lambda/4$ type III	2-gap, $\lambda/4$ type IV
Aperture diameter (mm)		30		
Geometrical beta, β_G	0.024	0.031	0.061	0.15
Beam steering compensation in the SRF cavity	No	No	No	Yes
Accelerating field (MV/m)	4.0	4.0	5.0	5.0
Synchronous phase (deg)	−30	−30	−30	−25
Random rms fluctuation of rf field phase (deg)	0.6	0.6	0.3	0.3
Random rms fluctuation of the field amplitude (%)	0.3	0.3	0.3	0.3
Effective length of solenoids (cm)	10	10	18	30
Type of solenoid	I	I	II	III
Length of focusing period (cm)	54.9	63.3	113.0	177.3
Focusing field (T)	7.0–8.2	8.5–9.1	6.0–11.0	8.2–10.2
rms misalignments of the ends of the solenoid (mm)	0.09	0.09	0.12	0.17
rms misalignments of the ends of the cavities (mm)	0.17	0.17	0.17	0.17

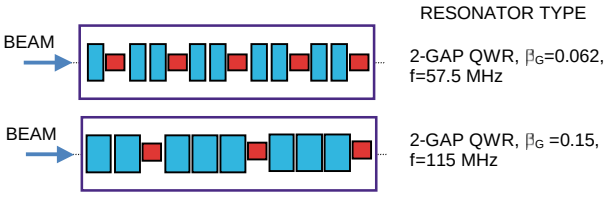

FIG. 3. (Color) Layout of the cryostats for two different types of cavities.

is designed for the cryostats containing 115 MHz SRF cavities.

rms and total beam envelopes of a two charge-state uranium beam along the low-β linac are shown in Fig. 4. Because of the perfect transverse matching there is no emittance growth even for a two charge-state uranium beam. The initial phase space distribution used for each charge state was the beam at the exit of the RFQ as simulated by the DYNAMION code [10]. Figure 5 shows the longitudinal phase space at the entrance of the SRF linac. Note that the longitudinal effective emittance of a 100% two charge-state uranium beam is 2.32 π keV/u nsec. In longitudinal phase space, the emittance of the two charge-state beam is always larger than for a single charge-state beam. Growth in effective emittance occurs due to the oscillations caused by the slightly differing off-tune synchronous phases for the two charge states 28^+ and 29^+. The effective emittance of a two charge-state beam oscillates along the linac as seen in Fig. 6. There are several obvious reasons for these oscillations: the synchronous phase for each sort of particle and mismatched motion due to intercryostat spaces. A frequency jump by a factor of 2 at 29.36 m does not introduce an additional emittance growth due to favorable beam parameters in this transition. Although the effective emittance value can be ~3.5 times larger than the input emittance, the total emittance of the two charge-state beam remains well inside the stable area in longitudinal phase space. The beam energy exiting the low-β section

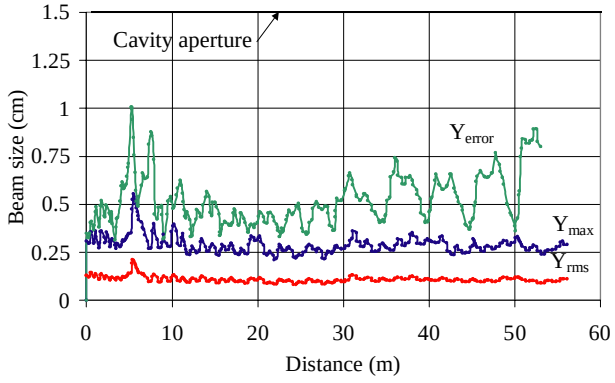

FIG. 4. (Color) Two charge-state beam rms ($Y_{\rm rms}$) and maximum ($Y_{\rm max}$) sizes in the vertical plane along the low-β linac. The red curve is the rms beam envelope, and the blue curve is the beam maximum envelope. The green curve ($Y_{\rm err}$) is the maximum beam size at given z due to misalignments obtained from 200 random seeds of the linac.

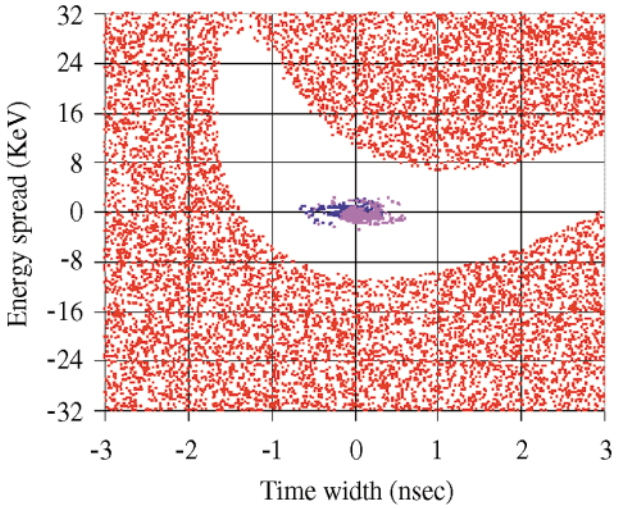

FIG. 5. (Color) Longitudinal acceptance of the low-β SRF linac. The blue and magenta dots show the longitudinal phase space plots of the uranium beam with charge $q = 28^+$ and $q = 29^+$ obtained at the RFQ exit.

should be selected in order to obtain the lowest effective emittance for the two charge-state beam. Obviously this feature is very important to maintain low emittance along the whole driver linac.

Effect of errors on beam parameters

All errors are randomly generated as a uniform distribution with the rms values δ_i listed in Table I. Accordingly the interval of the error distribution is $\pm\sqrt{3}\,\delta_i$. The sensitivity of multi-q beam parameters to various types of random errors and misalignments was studied by the ray-tracing code TRACK. The most essential errors affecting transverse beam motion are the misalignments of the transverse position of the focusing elements. Because of the strong defocusing of low velocity particles by the SRF cavities the misalignments of the SRF cavities were taken into account too. Monte Carlo simulations of the dynamics of multi-q beams in the presence of alignment errors have been performed. We introduced alignment errors by displacing separately both ends of each solenoid and SRF cavity in both X and Y by an amount in accordance with the displacement values given Table I. Then we tracked the multi-q beam through this portion of the linac and noted the increase in transverse emittance resulting from the positioning errors. As discussed in Refs. [6,7] the multi-q beam requires corrective steering in order to avoid appreciable emittance growth. Therefore our simulation was done in the presence of steering elements along the linac. The two charge-state beam deflection angle is measured and corrected by a one-element steering coil which is combined with a SC solenoid. Such steering occurs once in every third solenoid along the linac. This entire simulation was then repeated 200 times, each time with a different, random set of alignment errors. The code also calculates

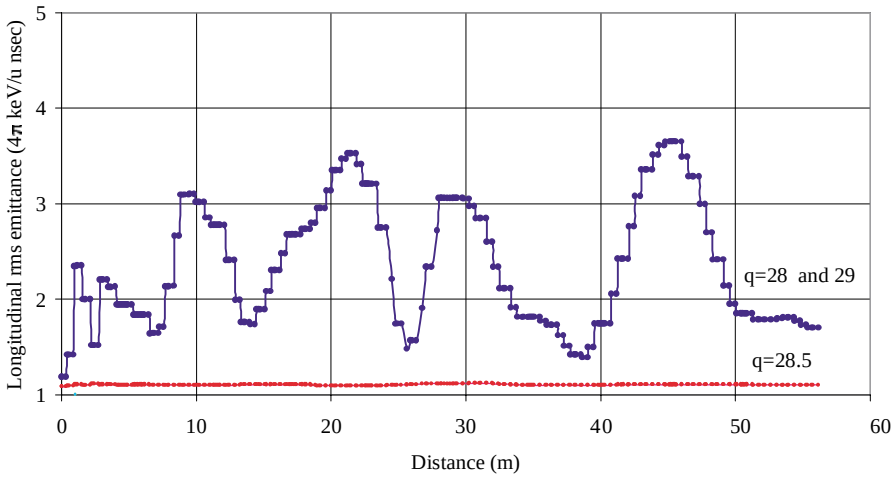

FIG. 6. (Color) rms longitudinal emittance variation of single (red curve) and two charge-state (blue curve) beams along the low-β linac.

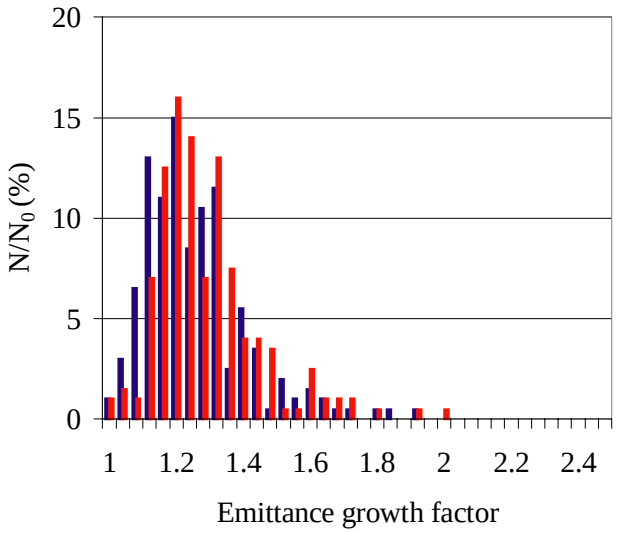

FIG. 7. (Color) Emittance growth in the misaligned focusing channel of the low-β linac with the steering correction. The vertical axis is a percentage of simulations with the indicated emittance growth, $N_0 = 200$. Blue and red bars show horizontal and vertical planes correspondingly.

TABLE II. Summary of longitudinal beam emittance at the exit of the low-β section.

Parameter	Emittance π keV/u nsec
4 rms emittance of a single charge-state beam	1.2
4 rms emittance of a two charge-state beam	1.7
4 rms emittance of a two charge-state beam with errors	1.9
98% emittance of a two charge-state beam accumulated during 200 random seeds	3.9
100% emittance of a two charge-state beam accumulated during 200 random seeds	10.0

maximum beam size for all 200 seeds at the given position along z. This beam envelope is shown in Fig. 4 by the green curve. As is seen, one-element steering keeps the beam within half of the aperture avoiding any additional emittance growth due to nonlinear focusing fields. The emittance growth factor is the ratio of normalized transverse emittance of the beam at exit to that at entrance. Figure 7 is a histogram of the results. The most probable effective emittance growth factor of the two charge-state beam is ~20% in both X and Y planes. In the worse case the emittance growth is just a factor of 2.

Errors of phase and amplitude fluctuations are simulated in order to find their effect on longitudinal effective emittance of the two charge-state beam. The error values listed in Table I are based on the experience of the ATLAS accelerator which is a 50 MV superconducting heavy-ion linac being operated at Argonne National Laboratory. Phase and

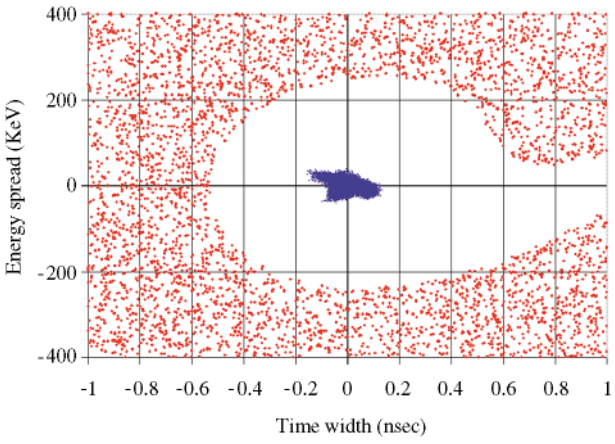

FIG. 8. (Color) Longitudinal acceptance of the medium-β SRF linac 7. The blue dots show the longitudinal phase space plots of the uranium beam with charge $q = 28^+$ and $q = 29^+$ accumulated during 200 seeds of the linac with random fluctuations of phases and amplitudes.

amplitude errors of the rf field are fast fluctuations and produce effective emittance growth of the multi-q beam. Table II summarizes the total effect of longitudinal emittance growth of the two charge-state beam in the low-β section with errors. Phase space plots obtained during 200 seeds are accumulated and shown in Fig. 8. As seen the emittance of the two charge-state beam remains much smaller than the acceptance of the following linac section.

IV. MEDIUM-β LINAC

Table III shows basic parameters of the medium-β section. This section contains two types of half-wave SRF cavities: 172.5 MHz 2-gap cavities and 345 MHz 3-gap spoke cavities. A nice feature of these cavities is the lack of any beam steering fields inside the beam aperture. The layout of the focusing and accelerating structure inside the cryostat is shown in Fig. 9. As in the low-β section, the focusing period in the front end of the cryostat misses a cavity. The total number of cryostats in the medium-β section is 26. The flange-to-flange distance between the elements located in adjacent cryostats is set to be 50 cm.

Simultaneous acceleration of a five charge-state uranium beam has been studied numerically. The simulation starts with a 9.2 MeV/u uranium beam equally distributed over five charge states, all at the same rf phase, and with a total normalized transverse emittance of 1.0 π mm mrad and total longitudinal emittance of ~ 10 π keV/u nsec. These values of emittances include the effect of errors in the upstream section of the linac. A waterbag initial phase space distribution for each charge state was generated for the given emittance values.

TABLE III. Basic parameters of the medium-β linac section.

Beam energy, MeV/u	9.2–43.6	43.6–85.2
Frequency (MHz)	172.5	345
Number of cavities per focusing period	3	4
Number of cavities	104	91
Number of cryostats	13	13
Type of cavity	2-gap, $\lambda/2$	3-gap, $\lambda/2$
Aperture diameter (mm)	30	
Geometrical beta, β_G	0.19	0.36
Synchronous phase (deg)	-30	$-30 \rightarrow -20$
Accelerating field (MV/m)	5.0	
Random rms fluctuation of the rf field phase (deg)	0.3	
Random rms fluctuation of the field amplitude (%)	0.3	
Effective length of solenoids (cm)	30	
Length of focusing period (cm)	173.4	258.9
Focusing field (T)	6.0–9.0	9.5–10.4
rms misalignments of the ends of the solenoid (mm)	0.17	
rms misalignments of the ends of the cavities (mm)	0.17	

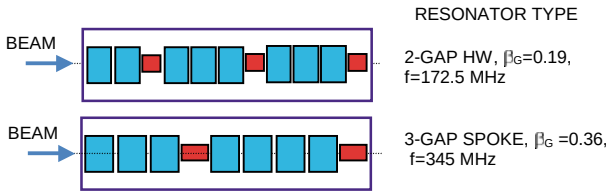

FIG. 9. (Color) Layout of the cryostats for two different types of cavities.

rms and total beam envelopes of the five charge-state uranium beam along the medium-β linac are shown in Fig. 10. The concept of the missing cavity at the first focusing period of the cryostats allows us to obtain very smooth matched envelopes along the linac as seen from Fig. 10. Because of the perfect matching there is no transverse emittance growth even for the five charge-state uranium beam. Figure 11 shows rms longitudinal emittance behavior along the accelerator. The synchronous phase is kept constant in the 172.5 MHz section. For better matching to the narrow phase acceptance of the 805 MHz section of the driver linac the synchronous phase is ramped along the 345 MHz section in the range from $-30°$ to $-20°$. As mentioned in Ref. [5] the tests of spoke cavities indicate the possibility to obtain higher accelerating gradients. High fields would make the longitudinal beam matching to the high-β section of the driver linac easier. As expected the longitudinal emittance of a single charge-state beam remains constant along the linac as seen in Fig. 11. However, the five charge-state beam emittance oscillates along the medium-β section and it is reasonable to select the stripping energy at the minimum of the longitudinal emittance (see Fig. 11). This energy is 85.3 MeV/u and results in an average charge state 89 of uranium beam after the carbon or lithium film stripper.

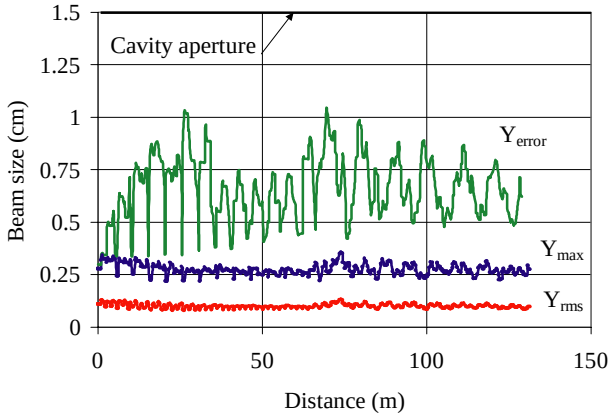

FIG. 10. (Color) A five charge-state beam rms (Y_{rms}) and maximum (Y_{max}) sizes in the vertical plane along the medium-β linac. The red curve is the rms beam envelope, and the blue curve is the beam maximum envelope. The green curve (Y_{err}) is the maximum beam size at given z due to misalignments obtained from 200 random seeds of the linac.

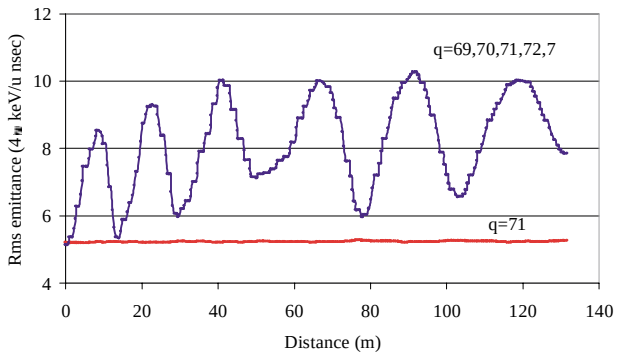

FIG. 11. (Color) rms longitudinal emittance variation of single and five charge-state uranium beams along the medium-β linac.

Effect of errors on beam parameters

The error study was performed with similar approaches applied to the low-β section of the linac. Particularly, a multi-q beam position is steered by the correctors located on the last solenoid of each cryostat. The results of the transverse emittance growth of the five charge-state uranium beam are shown in Fig. 12. The most probable effective emittance growth factor for a two charge-state beam is $\sim$20% in both the X and the Y planes. In the worse case the emittance growth is just a factor of 2.4. In this simulation, the five charge-state beam deflection angle is determined at the exit of each cryostat and corrected by a one-element corrector. The code also calculates the beam maximum size for all 200 seeds at the given position along z. This beam envelope is shown in Fig. 10. As seen, one-element steering keeps the beam well within the linac aperture. The corrective steering of a multi-q beam allows us to preserve the effective emittance at a very low level.

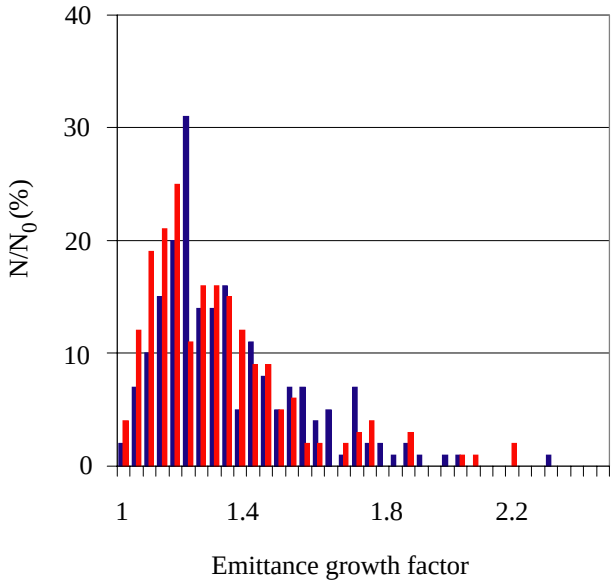

FIG. 12. (Color) Transverse emittance growth of a five charge-state uranium beam in the misaligned focusing channel of the medium-β linac. The vertical axis is a percentage of simulations with the indicated emittance growth, $N_0 = 200$. The blue and the red bars show horizontal and vertical planes correspondingly.

TABLE IV. Summary of longitudinal beam emittance at the exit of the medium-β section.

Parameter	Emittance π keV/u nsec
4 rms emittance of a single charge-state beam	5.26
4 rms emittance of a five charge-state beam	7.85
4 rms emittance of a five charge-state beam with errors	9.96
98% emittance of a five charge-state beam accumulated during 200 random seeds	16.2
100% emittance of a five charge-state beam accumulated during 200 random seeds	29.0

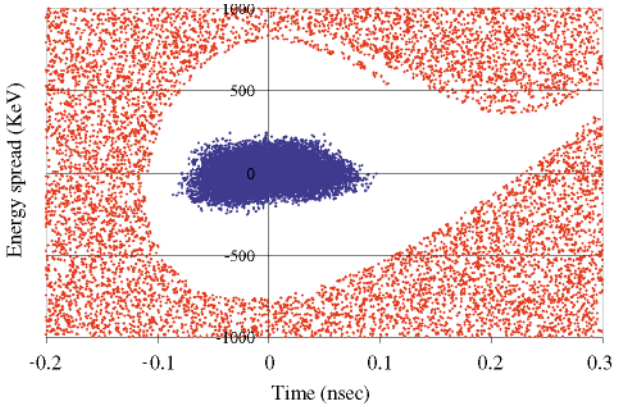

FIG. 13. (Color) Phase space plots of a five charge-state uranium beam at the location of the second stripper. The particle distribution (blue dots) fits into the emittance 29 π keV/u nsec. The red dots outline the acceptance of the linac section containing high-β 805 MHz SC elliptical cavities.

Errors of the accelerating field listed in Table III were applied in a simulation of the medium-β linac. Table IV summarizes the total longitudinal emittance growth of a five charge-state beam in the medium-β linac section with errors. Phase space plots obtained during 200 seeds are accumulated and shown in Fig. 13 together with the acceptance of the high-β section of the driver linac. As seen the emittance of a five charge-state beam is easily contained within the acceptance of the high-β section of the driver linac.

V. HIGH-β LINAC

The high-β section contains 136 cavities, only 33% of the total number of cavities in the RIA driver linac, but provides 76% of the accelerating voltage. This section uses three different types of 6-cell foreshortened elliptical cell cavities, all operating at a frequency of 805 MHz, and a temperature below 2 K [1,3,5]. The frequency is chosen to match the superconducting driver linac currently under construction for the Spallation Neutron Source (SNS) project. By operating at 805 MHz the RIA driver can

TABLE V. Basic parameters of the high-β linac section.

Energy range (MeV/u)	81–154	154–326	326–404
Geometrical beta	0.49	0.61	0.81
Accelerating gradient (MV/m)	10.54	13.01	15.99
Cavity peak surface field (MV/m)		35.0	
Cavity length (cm)	55	68	91
Cryomodule length (m)	2.5	5.2	6.3
Number of cavities	48	64	24
Focusing lattice		FDO	
rms fluctuation of rf field phase (deg)		0.3	
rms fluctuations of the field amplitude (%)		0.3	
Number of focusing periods	16	16	6
Length of quadrupole (cm)	25	41	41
Length of the focusing period (m)	3.65	5.84	7.89
Focusing gradient (T/m)	12.0–20.0	12.0–14.0	15.0
rms misalignments of the ends of quadrupoles (mm)		0.1	

use the $\beta_G = 0.61$ and $\beta_G = 0.81$ cavities and cryomodules being developed for SNS, leaving only the $\beta_G = 0.49$ elliptical cavity to be developed specifically for RIA. Table V presents the main parameters of the accelerating cavities and focusing lattice of the high-β section.

At most the high-β linac will contain four SC cavities per cryostat. However, in the beginning of the high-β section the focusing must be strong enough in order to avoid a coupling between the longitudinal and transverse motions. The latter, as was found from the beam dynamics simulation, can cause appreciable transverse emittance growth. Therefore the first 16 cryomodels are relatively short and contain three $\beta_G = 0.49$ elliptical cavities. The focusing elements will be placed in between the cryostats, in the form either of normal-conducting quad doublets or SC solenoids. The SC solenoids can be placed in separate

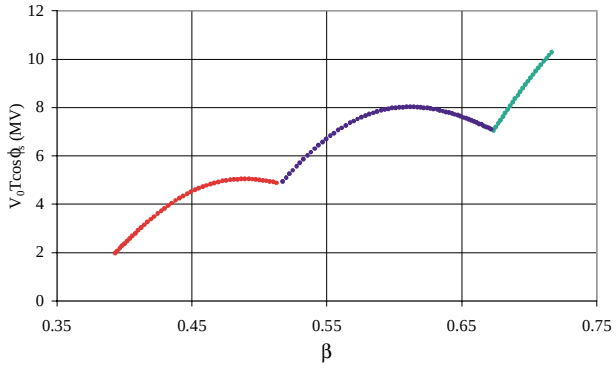

FIG. 14. (Color) Voltage gain of the uranium beam in the high-β 805 MHz SC elliptical cavities. The colors represent three different types of cavities.

TABLE VI. Summary of longitudinal beam emittance at the exit of the driver linac.

Parameter	Emittance π keV/u nsec
4 rms emittance of a single charge-state beam	13.6
4 rms emittance of a four charge-state beam	13.6
4 rms emittance of a four charge-state beam with errors	18.2
98% emittance of a four charge-state beam accumulated from 200 random seeds	33.5
100% emittance of a four charge-state beam accumulated during 200 random seeds	75.8

cryostats. Table V shows parameters of the focusing lattice for the option with quadrupole focusing.

The accelerating gradients in elliptical cavities are expected to be rather high. Already the SNS $\beta_G = 0.81$ cavities are assumed to obtain a 35 MV/m peak surface field. Assuming further improvement of SRF technology we accept this number for all types of elliptical cavities. The accelerating voltage for the velocity profile of the uranium beam is shown in Fig. 14.

A beam dynamics simulation of a four charge-state uranium beam including errors of phase and amplitude of the rf field was done for the high-β section. The range of errors is listed in Table V. Four charge states, 88, 89, 90, and 91, have been tracked simultaneously through the linac section 200 times, each time with separately seeded errors of the accelerating field. The results of this simulation are summarized in Table VI and Fig. 15. The latter shows longitudinal phase space plots accumulated during 200 random seeds. As seen the multi-q uranium beam can be accelerated up to 400 MeV/u within $\pm 0.25\%$ of energy spread and remains within $\pm 10°$ phase width. Longitudinal emittance 75.8 π keV/u nsec contains all particles shown in Fig. 15.

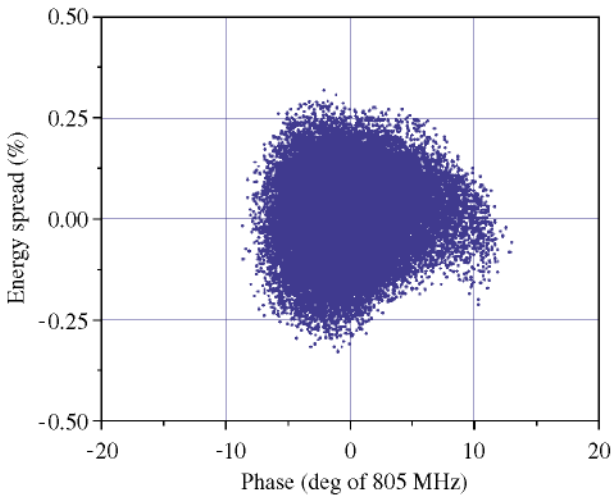

FIG. 15. (Color) Phase space plots of a four charge-state uranium beam at the exit of the driver linac.

Warm quadrupole magnets can be aligned with a precision ~ 100 μm of rms deviation from the accelerator axis. In the high-β section the beam center can be easily corrected, and the multiplicity of the charge state does not produce any additional emittance growth.

VI. STRIPPER SECTIONS

The driver linac requires two charge-stripping sections. The passage of the high intensity heavy-ion beam through the stripping film or foil results in several effects.

(i) At the exit of the stripping foil, the ion beam is a mixture of several charge states, the intensities of which are a Gaussian distribution.

(ii) The stripping foil experiences a high thermal load, especially at the first stripper. A liquid lithium film for the first stripper is under development [18], both to accommodate the thermal load and also to produce higher charge states.

(iii) The average energy of the ion beam is slightly decreased due to ionization losses in the stripper.

(iv) The transverse and longitudinal beam emittances are increased due to the energy straggling and scattering.

Table VII shows the effect of the stripper on the uranium beam [19]. In order to avoid beam losses in the high-energy section of the driver linac the low intensity unwanted charge states must be carefully separated and dumped. As long as the driver linac is designed for the acceleration of multi-q beams, the beam transport system following the stripping foil must provide simultaneous matching of selected charge states to six-dimensional acceptance of the following SRF linac [20]. This magnetic transport system (MTS) requires dipole magnets and a rebuncher in order to provide a proper transformation of the six-dimensional beam emittance. The system must have a dispersive area, effectively operating as a spectrometer. In the region of maximum dispersion, the unwanted charge states are removed by horizontal beam collimation. We have designed such systems for both stripping areas. Several options for the MTS design can satisfy the above requirements. The options chosen seem to best satisfy the overall architectural requirements of the linac. For example, after the first stripper, it is convenient to transversely shift the linac beam axis: the MTS incorporates two 90° bends to provide a 4.5 m shift.

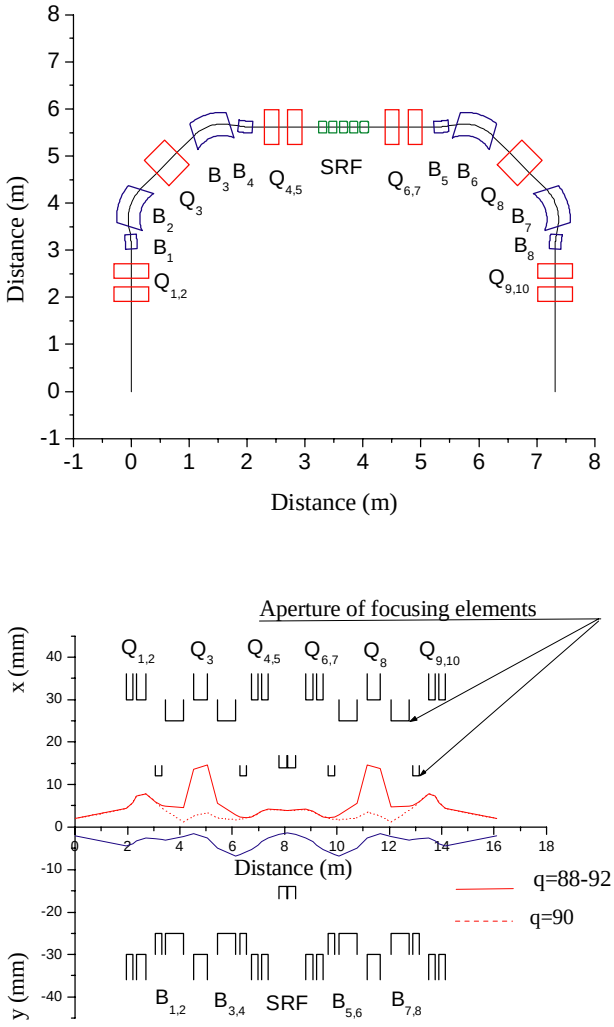

FIG. 16. (Color) System for selecting multiple q state beams through a 180° bend at 81 MeV/u (top figure). Plot of envelopes (bottom figure).

After the second stripper it is economical to bend the beam through 180°, since such a bend greatly shortens the overall length of the linac tunnel. The 180° bend provides for high dispersion regions in the MTS which enable separation of low intensity charge states and cleaning or scraping of any beam halo.

For simplicity of the MTS design, we assume the beam matrix of the second moments must be the same at the

TABLE VII. Stripper effect on the uranium beam.

Beam energy (MeV/u)	9.43	85.2
Medium	Liquid lithium film	Rotating carbon wheel
Thickness (mg/cm^2)	0.1	15
Energy loss (MeV/u)	0.01	4.0
Mean charge state	71	89
Charge states	69–73	88–91
Beam fraction within design charge states (%)	69	96
rms angle of transverse beam scattering (mrad)	0.2	0.44
rms energy spread (keV/u)	4.1	13.5

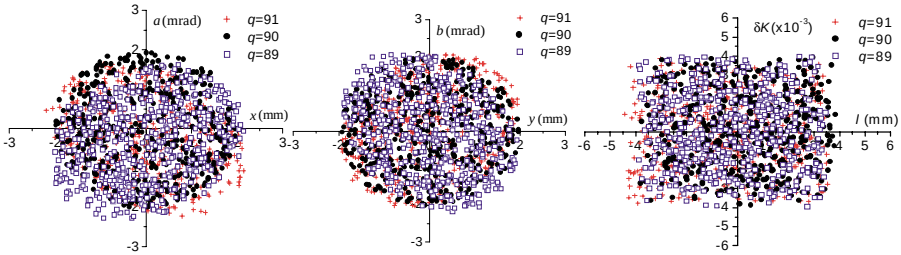

FIG. 17. (Color) Plots of particles occupying the x-a, y-b, and l-dK phase space at the exit of the 180° bend system (left to right). The selected charge states are $q = 89$, 90, and 91 and the calculation was carried out to third order.

entrance and at the exit of the system. The preliminary design of the MTS has been done assuming zero longitudinal emittance. For our purpose the MTS must provide the same path length for each of the multiple charge states so that the net effect on the longitudinal phase space is the same as a simple drift space. The reproduction of the second order moments of the beam in the longitudinal phase space is provided for by the rf cavity, a 345 MHz SRF cavity operating as a rebuncher, which must be located in a zero dispersion area. All bunches of a different charge state must arrive at the rf cavity at the same time (at the same phase of the rf field). This means that the MTS must have the same path length for all charge states in the initial portion, up to the rebuncher, and also, separately, in the output portion from the rebuncher on. At the final stage of the MTS design, the higher order terms must be included and corrected as necessary. For this final design stage, numerical simulations of the beam through the MTS were performed including the rebuncher and assuming realistic, nonzero initial emittances in all phase planes. Beam simulation for the design process was performed using the code COSY [13].

As an example in Fig. 16 we show one of the MTS, which follows the second stripper. Following the second stripper, for a uranium beam, charge states $q = 88$, 89, 90, and 91 will continue on through the system. The transport channel has been designed for the beam parameters obtained in Sec. IV of this paper.

The design sequence for the MTS follows.

(i) The distance between the magnets B_1 and B_2 was adjusted in order to make the path length for all charge states the same.

(ii) The gradient in the quadrupole Q_3 was adjusted to make the bend through the magnets B_1, B_2, B_3, and B_4 achromatic.

Meeting these conditions insures that the trajectory length is independent of the initial beam parameters. Therefore the longitudinal phase space beam optics in the section from the entrance to the rf cavity are equivalent to a simple drift. The rf cavity field is adjusted in order to keep the average energy for the different charge states constant and to obtain the same phase space portrait of the beam at the exit of the MTS as at the entrance. The gradients in Q_1, Q_2, Q_3, and Q_4 are fitted in order to obtain transformation matrices equal to the unit matrix in the horizontal plane and the minus unit matrix in the vertical plane. Beam envelopes along the MTS are shown in Fig. 16. The dispersion function D is maximum at the entrance of the lens Q_3. The proposed design of the MTS provides transverse spatial separation of the different charge states of the beam at the entrance of the lens Q_3, as shown in Fig. 16.

The proposed transport system provides unit transformation of beam emittances as shown in Fig. 17. There is no appreciable emittance growth for the three charge-state beam even if calculations include third order terms. However, for the transformation of a larger number of charge states the transport system must be designed with the correction of higher order terms.

VII. CONCLUSION

We have continued to develop and improve the baseline design for the medium-energy entirely SC heavy-ion linac. Several novel features have been implemented into the baseline design. A detailed beam dynamics simulation has been performed for a multi-q uranium beam from the source to the linac exit. These simulations have been iterated repeatedly with the design of the overall linac architecture. The simulations, which include misalignments of focusing and accelerating elements and random errors of the rf fields, show that beam emittances are well below the six-dimensional acceptance throughout the whole SC linac.

ACKNOWLEDGMENT

This work was supported by the U.S. Department of Energy, Nuclear Physics Division, under Contract No. W-31-109-ENG-38.

[1] K. W. Shepard, J. R. Delayen, C. M. Lyneis, J. A. Nolen, P. N. Ostroumov, J. W. Staples, J. Brawley, C. Hovater, M. Kedzie, M. P. Kelly, J. Mammosser, C. Piller, and M. Portillo, in *Proceedings of the 9th International Workshop of RF Superconductivity, Santa Fe, 1999,* edited by B. Rusnak (LANL, Los Alamos, 2000), p. 345.

[2] P. N. Ostroumov, K. W. Shepard, J. A. Nolen, and R. C. Pardo, in ICFA Beam Dynamics Newsletter, No. 20, August, 1999, p. 60.
[3] C. W. Leemann, in *Proceedings of the XXth International Linac Conference, Monterey, California, 2000*, edited by A. W. Chao (Report No. SLAC-R-561), p. 331.
[4] G. Savard, in *Proceedings of the 2001 Particle Accelerator Conference, Chicago, IL, 2001*, edited by P. Lucas and S. Webber (IEEE, Piscataway, NJ, 2001), p. 561.
[5] K. W. Shepard, in Proceedings of the 10th International Workshop on RF Superconductivity, Tsukuba, Japan, 2001 (to be published), Paper TA003 (http://conference.kek.jp/SRF2001/).
[6] P. N. Ostroumov, J. A. Nolen, and K. W. Shepard, in *Proceedings of the XXth International Linac Conference, Monterey, California, 2000* (Ref. [3]), p. 1018.
[7] P. N. Ostroumov and K. W. Shepard, Phys. Rev. ST Accel. Beams **3**, 030101 (2000).
[8] P. N. Ostroumov, R. C. Pardo, G. P. Zinkann, K. W. Shepard, and J. A. Nolen, in *Proceedings of the XXth International Linac Conference, Monterey, California, 2000* (Ref. [3]), p. 205.
[9] P. N. Ostroumov, R. C. Pardo, G. P. Zinkann, K. W. Shepard, and J. A. Nolen, Phys. Rev. Lett. **86**, 2798–2801 (2001).
[10] P. N. Ostroumov, K. W. Shepard, V. N. Aseev, and A. A. Kolomiets, in *Proceedings of the XXth International Linac Conference, Monterey, California, 2000* (Ref. [3]), p. 202.
[11] M. A. Leitner, D. C. Wutte, and C. M. Lyneis, in *Proceedings of the 2001 Particle Accelerator Conference, Chicago, IL, 2001* (Ref. [4]), p. 67.
[12] H. Wollnik, J. Brezina, and M. Berz, Nucl. Instrum. Methods Phys. Res., Sect. A **258**, 408 (1987).
[13] M. Berz, COSY INFINITY, MSU, 1999.
[14] A. A. Kolomiets, V. Pershin, I. Vorobyov, S. Yaramishev, and Ju. Klabunde, in *Proceedings of the Sixth European PAC, Stockholm, Sweden, 1998*, edited by S. Myers *et al.* (IOP, Bristol, U.K., 1998), p. 1201.
[15] P. N. Ostroumov and K. W. Shepard, Phys. Rev. ST Accel. Beams **11**, 030101 (2001).
[16] K. L. Brown, SLAC Report No. 91, 1979.
[17] CST Microwave Studio, CST GmbH, Darmstadt, Germany, 2001 (http://www.cst.de/).
[18] J. Nolen, C. B. Reed, A. Hassanein, M. Portillo, and J. H. Norem, in ANL Physics Division Annual Report 2000, No. ANL-01/19, 2001, p. 152.
[19] M. Portillo (private communication).
[20] M. Portillo, V. N. Aseev, J. A. Nolen, and P. N. Ostroumov, in *Proceedings of the 2001 Particle Accelerator Conference, Chicago, IL, 2001* (Ref. [4]), p. 3012.